



Microstructure Model for Welding Simulations

Final Report 278-T-08

for Project

Development of Optimized Welding Solutions for X100 Line Pipe Steel

Prepared for the

Design, Materials, and Construction Technical Committee of
Pipeline Research Council International, Inc.
Project MATH-1 Catalog No. L5XXXX

and

U.S. Department of Transportation
Pipeline and Hazardous Materials Safety Administration
Office of Pipeline Safety
Agreement Number DTPH56-07-T-000005

Prepared by

Yaoshan Chen and Yong-Yi Wang, CRES
Marie Quintana and V.B. Rajan, LECO
Jim Gianetto, CANMET

September 2011

This research was funded in part under the Department of Transportation, Pipeline and Hazardous Materials Safety Administration's Pipeline Safety Research and Development Program. The views and conclusions contained in this document are those of the authors and should not be interpreted as representing the official policies, either expressed or implied, of the Pipeline and Hazardous Materials Safety Administration, or the U.S. Government.



Catalog No. L5XXXX

Microstructure Model for Welding Simulations

Final Report 278-T-08

for Project

Development of Optimized Welding Solutions for X100 Line Pipe Steel

Prepared for the

Design, Materials, and Construction Technical Committee of
Pipeline Research Council International, Inc.
Project MATH-1 Catalog No. L5XXXX

and

U.S. Department of Transportation
Pipeline and Hazardous Materials Safety Administration
Office of Pipeline Safety
Agreement Number DTPH56-07-T-000005

Prepared by

Yaoshan Chen and Yong-Yi Wang, CRES
Marie Quintana and V.B. Rajan, LECO
Jim Gianetto, CANMET

September 2011

Version	Date of Last Revision	Date of Uploading	Comments
07	4-29-2011	4-29-2011	After PRCI Review
08	09-01-2011	09-01-11	Final

This report is furnished to Pipeline Research Council International, Inc. (PRCI) under the terms of PRCI contract [278-PR- 348 - 074513], between PRCI and the MATH-1 contractors:

- Electricore (prime contractor),
- Center for Reliable Energy Systems, CANMET, NIST, and The Lincoln Electric Company (sub-contractors).

The contents of this report are published as received from the MATH-1 contractor and subcontractors. The opinions, findings, and conclusions expressed in the report are those of the authors and not necessarily those of PRCI, its member companies, or their representatives. Publication and dissemination of this report by PRCI should not be considered an endorsement by PRCI of the MATH-1 contractor and subcontractors, or the accuracy or validity of any opinions, findings, or conclusions expressed herein.

In publishing this report, PRCI and the MATH-1 contractors make no warranty or representation, expressed or implied, with respect to the accuracy, completeness, usefulness, or fitness for purpose of the information contained herein, or that the use of any information, method, process, or apparatus disclosed in this report may not infringe on privately owned rights. PRCI and the MATH-1 contractors assume no liability with respect to the use of, or for damages resulting from the use of, any information, method, process, or apparatus disclosed in this report. By accepting the report and utilizing it, you agree to waive any and all claims you may have, resulting from your voluntary use of the report, against PRCI and the MATH-1 contractors.

Pipeline Research Council International Catalog No. L5XXXX

PRCI Reports are Published by Technical Toolboxes, Inc.

3801 Kirby Drive, Suite 520
Houston, Texas 77098
Tel: 713-630-0505
Fax: 713-630-0560
Email: info@ttoolboxes.com

PROJECT PARTICIPANTS			
PROJECT TEAM MEMBER	COMPANY AFFILIATION	PROJECT TEAM MEMBER	COMPANY AFFILIATION
Arti Bhatia	Alliance	Jim Costain	GE
Jennifer Klementis	Alliance	Gilmar Batista	Petrobras
Roger Haycraft	Boardwalk	Marcy Saturno de Menezes	Petrobras
David Horsley	BP	Dave Aguiar	PG&E
Mark Hudson	BP	Ken Lorang	PRCI
Ron Shockley	Chevron	Maslat Al-Waranbi	Saudi Aramco
Sam Mishael	Chevron	Paul Lee	SoCalGas
David Wilson	ConocoPhillips	Alan Lambeth	Spectra
Satish Kulkarni	El Paso	Robert Turner	Stupp
Art Meyer	Enbridge	Gilles Richard	TAMSA
Bill Forbes	Enbridge	Noe Mota Solis	TAMSA
Scott Ironside	Enbridge	Philippe Darcis	TAMSA
Sean Keane	Enbridge	Dave Taylor	TransCanada
Laurie Collins	Evraz	Joe Zhou	TransCanada
David de Miranda	Gassco	Jason Skow	TransGas
Adriaan den Herder	Gasunie	Ernesto Cisneros	Tuberia Laguna
Jeff Stetson	GE	Vivek Kashyap	Welpsun
		Chris Brown	Williams

CORE RESEARCH TEAM	
RESEARCHER	COMPANY AFFILIATION
Yaoshan Chen	Center for Reliable Energy Systems
Yong-Yi Wang	Center for Reliable Energy Systems
Ming Liu	Center for Reliable Energy Systems
Dave Fink	Lincoln Electric Company
Marie Quintana	Lincoln Electric Company
Vaidyanath Rajan	Lincoln Electric Company
Joe Daniel	Lincoln Electric Company
Radhika Panday	Lincoln Electric Company
James Gianetto	CANMET Materials Technology Laboratory
John Bowker	CANMET Materials Technology Laboratory
Bill Tyson	CANMET Materials Technology Laboratory
Guowu Shen	CANMET Materials Technology Laboratory
Dong Park	CANMET Materials Technology Laboratory
Timothy Weeks	National Institute of Standards and Technology
Mark Richards	National Institute of Standards and Technology
Dave McColskey	National Institute of Standards and Technology
John Hammond	Consultant Metallurgist & Welding Engineer

This Page Intentionally Left Blank

FINAL REPORT STRUCTURE

Focus Area 1 - Update of Weld Design, Testing, and Assessment Procedures for High Strength Pipelines		
Report #	Description	Lead Authors
277-T-01	Background of Linepipe Specifications	CRES/CANMET
277-T-02	Background of All-Weld Metal Tensile Test Protocol	CANMET/Lincoln
277-T-03	Development of Procedure for Low-Constraint Toughness Testing Using a Single-Specimen Technique	CANMET/CRES
277-T-04	Summary of Publications: Single-Edge Notched Tension SE(T) Tests	CANMET
277-T-05	Small Scale Tensile, Charpy V-Notch, and Fracture Toughness Tests	CANMET/NIST
277-T-06	Small Scale Low Constraint Fracture Toughness Test Results	CANMET/NIST
277-T-07	Small Scale Low Constraint Fracture Toughness Test Discussion and Analysis	CANMET/NIST
277-T-08	Summary of Mechanical Properties	CANMET
277-T-09	Curved Wide Plate Tests	NIST/CRES
277-T-10	Weld Strength Mismatch Requirements	CRES/CANMET
277-T-11	Curved Wide Plate Test Results and Transferability of Test Specimens	CRES/CANMET
277-S-01	Summary Report 277 Weld Design, Testing, and Assessment Procedures for High Strength Pipelines	CRES

Focus Area 2 - Development of Optimized Welding Solutions for X100 Linepipe Steel		
Report #	Description	Lead Authors
278-T-01	State of The Art Review	Lincoln
278-T-02	Material Selection, Welding and Weld Monitoring	Lincoln/CANMET
278-T-03	Microstructure and Hardness Characterization of Girth Welds	CANMET/Lincoln
278-T-04	Microstructure and Properties of Simulated Weld Metals	CANMET/Lincoln
278-T-05	Microstructure and Properties of Simulated Heat Affected Zones	CANMET/Lincoln
278-T-06	Essential Welding Variables	Lincoln/CANMET
278-T-07	Thermal Model for Welding Simulations	CRES/CANMET
278-T-08	Microstructure Model for Welding Simulations	CRES/CANMET
278-T-09	Application to Other Processes	Lincoln/CANMET
278-S-01	Summary Report 278 Development of Optimized Welding Solutions for X100 Line Pipe Steel	Lincoln

EXECUTIVE SUMMARY

This report was prepared by the Center for Reliable Energy Systems (CRES) for the DOT/PRCI co-sponsored project DTPH56-08-T-000005, “Development of Optimized Welding Solutions for X100 Line Pipe Steels.”

As part of the project in Tasks 2, “Identification of Essential Variables”, and Task 3, “Fundamental Understanding of Welding Processes and Essential Variables”, an integrated thermal and microstructure model has been developed to simulate the heat transfer and microstructure changes in gas-metal-arc-welding (GMAW) girth welds. This report summarized the microstructure simulation results produced by this integrated numerical model.

The numerical model employed a two-dimensional, axis-symmetrical finite element procedure to simulate the transient heat transfer process and the microstructure evolution both in the weld metal and the heat-affected-zone (HAZ). It not only covered the traditional single wire GMAW process, but also has the capabilities to analyze new GMAW processes such as tandem wire and dual torch.

Developed and implemented together with the thermal model, the microstructure model was first validated against the experimental measurements of hardness by Mark Hudson^[1]. A detailed comparison between the microstructure predictions of the model with a set of HAZ microstructure Gleeble test data was conducted. Furthermore, the model predictions of hardness were compared to the hardness measurements of the girth welds and experimental plate welds. Together with the thermal model, the microstructure model was used in the virtual experiments to identify essential welding variables.

The comparison between the experimental results and the numerical results proved that the microstructure model was capable of predicting the trend of hardness variation as a function of welding procedure, welding parameters, and chemical compositions of pipe materials and the weld metal. In developing the microstructure model, it was realized that with better and quantitative understanding of the mechanisms of microstructure responses to reheating welding cycles with different peak temperatures, in particular by those of inter-critical and sub-critical regions, the accuracy of hardness predictions by the microstructure for weld metal and HAZ could be greatly improved.

Acknowledgement

This work was jointly funded by PRCI and the U.S. Department of Transportation, Pipeline and Hazardous Materials Safety Administration (PHMSA)’s Pipeline Safety Research and Development. CRES would like to gratefully acknowledge the valuable supports and suggestions received from its project partners: Lincoln Electric, CANMET, BP, and TransCanada. The authors wish to thank Dr. Mark Hudson for granting permission to use his experimental test data and materials in his excellent Ph. D. Thesis.

Table of Contents

Table of Contents

Table of Contents	viii
Table of Contents	viii
List of Figures	ix
List of Tables	ix
1 Introduction	1
1.1 Background	1
1.2 Microstructure Simulation of GMAW	2
1.3 Objectives and Work Plan	3
1.4 Work Plan	3
2 Technical Approach and Implementation of Microstructure Model	4
2.1 Technical Approach for Microstructure Model	4
2.2 Numerical Implementation of Microstructure Model	6
3 Verification and Applications of Microstructure Model	6
3.1 Verification of Microstructure with Hudson’s Hardness Data	7
3.2 Verification of Microstructure Model with HAZ Gleeble Simulation Data	11
3.3 Verification of Microstructure Model with Plate Welds and Girth Welds	12
3.4 Virtual Experiments and Identification of Essential Variables	15
4 Concluding Remarks	16
4.1 Thermal-Microstructure Modeling of Multi-Pass, Multi-Wire P-GMAW Process	16
4.2 The Integrated Thermal-Microstructure Analysis Tool	16
5 References	17

List of Figures

Figure 1: Measured and computed hardness distributions along the weld centerline for different preheat temperatures.	8
Figure 2: Hardness contours for different preheat temperatures. Top left: no preheat; top right: 100oC preheat; bottom left: 180oC preheat.....	9
Figure 3: Transverse distributions of hardness along the centerline of girth weld for single wire, tandem wire, and dual torch processes.	10
Figure 4: Hardness contours for different processes. Top left: single wire; top right: tandem wire; bottom left: dual torch.	10
Figure 5: Gleeble simulation thermal cycle with $T_{85}=1.2s$	11
Figure 6: Predicted hardness distribution for plate weld.	13
Figure 7: Measured and predicted hardness profiles along weld centerline for plate weld.....	13
Figure 8: Measured micro-hardness (left) vs. predicted hardness distribution (right) in a girth weld.....	14

List of Tables

Table 1: Representative chemical composition of weld metal for pre-heat and process variation trials ^[1]	7
Table 2: Chemical composition of X100 pipe for pre-heat variation trials[1].	8
Table 3: Chemical composition of X100 pipe for process variation trials ^[1]	9
Table 4: Comparison of microstructure properties between HAZ Gleeble test and predictions by HAZ microstructure model (VF: volume fraction)	11
Table 5: Averaged welding parameters for plate weld	12
Table 6: Chemical composition of consumable PT1	12
Table 7: Chemical compositions of X100 pipe and weld metal.	14
Table 8: Averaged welding parameters for the girth weld.	14

1 Introduction

1.1 Background

Welding of micro-alloyed, high strength steels such as X100 poses a number of challenges due to, in part, the sensitivity of weld mechanical properties to the welding parameters such as heat input, preheat temperature, etc. For design purpose, it is often required that the mechanical properties of the welds overmatch those of the pipe materials in terms of yield strength, ductility, and toughness. In general, high strength pipe steels exhibit lower strain hardening capability, lower ductility, and increased anisotropy than the traditional lower grade steels. For these steels, when exposed to welding process, the heat-affected zone (HAZ) in the base metal can be softened and strain localization can take place. For weld metal, it is even more difficult to maintain a balance of ductility and fracture toughness at high strength because the weld metal performance is highly sensitive to welding parameters in comparison with lower strength steels.

Gas metal arc welding (GMAW) processes have become the popular choices for pipeline construction. In recent years, a number of high-productivity variants of GMAW such as tandem wire and dual torch have been employed for field welding in order to increase welding productivity. These new GMAW variants introduce more welding variables and further complicate the relationship between weld mechanical properties and welding conditions.

In principle, the mechanical properties of both weld metal and its HAZ are determined by their final microstructure after a series of phase transformations under the welding thermal cycles. The kinetics of the phase transformations, the final constituents and grain structure of the microstructure depend on the chemical compositions of both pipe materials and the welding consumables and the thermal cycles they are subjected to. In the case of X100 welding, the combination of new alloying design of welding consumables and high-productivity GMAW variants presents a new challenge in understanding the dependency of weld performance on welding procedures, parameters, and materials.

To date, the welding research related to X100 line pipe steel has been sponsored by a few major pipeline companies in collaboration with pipe manufacturers, Pipeline Research Council International (PRCI), universities, and government agencies from around the world. Some of this early research was conducted at Cranfield University, Edison Welding Institute (EWI), The Welding Institute (TWI), and CANMET. In particular, a comprehensive investigation was performed by Hudson^[1].

In order to understand the relationship between the mechanical properties of the weldment and the welding conditions, an effective approach is to simulate the thermal and microstructure processes in GMAW processes. By predicting the thermal cycles and the phase transformations, the microstructure of both weld metal and its HAZ can be determined numerically. With the assistance of experimental measurements, it is possible to identify the welding essential variables and evaluate their influences on the final weld performance. For this reason, an integrated thermal-microstructure model was developed in the project. The

in-depth discussion of the thermal model was presented in a separate technical report^[2]. This report will cover the microstructure model only.

1.2 Microstructure Simulation of GMAW

Over the past decades, there have been numerous research efforts to investigate the relationship between welding conditions and the final mechanical properties of the weld. A number of empirical relations have been formulated for correlation of weld HAZ hardness, chemical compositions, and cooling rates^[3,4,5]. Microstructure models that are capable of simulating phase transformation and determining hardness in metals given their chemical compositions and the thermal cycles have also been developed. The early works by Kirkaldy and Venugopalan^[6] showed that phase transformation in metals with relatively low alloying elements can be modeled with a rate-based kinetics algorithm. This general kinetics algorithm was later modified and extended to cover wider alloying ranges^[7] and other phase transformation processes during welding under continuous cooling conditions. Watt et al., for example, developed a numerical algorithm based on Kirkaldy's model for the microstructure development in HAZ^[8]. In an effort to predict microstructure and hardness in HAZ with multi-thermal-cycle, Oddy et al. combined the Kirkaldy algorithm with proposed mechanisms for carbon segregation, re-austenization^[9], and tempering effects^[10]. Borjesson and Lindgren^[11] used the Kirkaldy algorithm to predict the microstructure of multi-pass welds not only for HAZ but also for weld metal. Bhadeshia developed theoretical and numerical approaches toward microstructures of weld metal from a number of perspectives^[12]. The latest industrial research work on microstructure and hardness prediction for multi-pass girth weld was by Nunzio et al.^[13], where an analytical approach based on phase transformation kinetics and an artificial neural network approach based on selected database of continuous cooling (CCT) diagrams were developed. Early works by the present authors focused on the predictions of microstructure and hardness in weld HAZ^[14].

Microstructure modeling of welding processes has been a diverse research area because of the variety of welding processes and materials involved. In general, the weld metal and its HAZ are treated differently due to their marked differences in chemical compositions, grain structures, and, to certain extent, phase transformations. For the modeling and simulation of HAZ, there were many microstructure models, analyses, and correlations such as Kirkaldy^[6], Yurioka's^[3] and others^[15,16]. These models were based on either a metallurgy-based phase transformation kinetics theory or an engineering correlation approach. From these models, a measurable mechanical property, mostly the hardness value, can be predicted. For the weld metal, on the other hand, the modeling efforts, such as those by Bhadeshia^[12], have been focused on the understanding of phase transformation in welds and other unique features associated with welding processes such as effects of non-metallic inclusions. There are a very limited number of models where weld metal hardness was evaluated in a consistent framework. Consequently, some of the weld metal models utilized the microstructure algorithm by Kirkaldy to calculate the hardness values for weld metal. As one of the outputs of these microstructure models, hardness was chosen due to two primary reasons: 1) it is a measurable mechanical property for steels and 2) for steels; it has constantly demonstrated excellent correlation with tensile strength.

1.3 Objectives and Work Plan

1.3.1 Objectives

As a part of the project, an analysis tool was needed to predict the thermal cycles and microstructures of the weld metal and HAZ regions. For this purpose, an integrated thermal-microstructure finite element model was developed. With the background and the current status of microstructure modeling for welding processes, the microstructure model was developed to predict the constituents and overall hardness values in HAZ and weld metal. Together with the thermal model, the microstructure model served multiple purposes during the overall execution of the project:

- 1) Help understand the effects of welding parameters, including those related to multi-wire P-GMAW processes;
- 2) Help identify the essential variables of X100 welding process through virtual experiments;
- 3) Help welding procedure design, perform results predictions, and evaluate welding results.

During its development, the microstructure model was embedded in the thermal model. It shares much of the application scope of the thermal model. Like the thermal model, the microstructure model was developed in different formats, verified against a number of measurement data sets, and finally became part of a stand-alone software analysis tool.

1.4 Work Plan

In developing the microstructure model, a number of steps were taken to establish the simulation procedure, calibrate and verify the model, and perform virtual experiments and welding result predictions. These steps include:

- 1) Development and verification of the microstructure model with ABAQUS, a commercial finite element package;
- 2) Implementation of the microstructure model in a stand-alone analysis software tool;
- 3) Calibration and verification of the microstructure model with HAZ Gleeble simulation data;
- 4) Calibration and verification of the microstructure model with weld metal Gleeble simulation data;
- 5) Virtual experiments and identifications of essential variables;
- 6) Simulation and prediction of plate welding results.

Overall the microstructure model was developed and implemented together with the thermal model; the thermal model took precedence in overall model structure design and implementation. Consequently, the microstructure model followed the thermal model in work flow as described in the topical report for the thermal model, Report 278-T-07^[2].

2 Technical Approach and Implementation of Microstructure Model

In this section, the technical approach for the development of the microstructure model is first presented. As stated in the previous section, the development and verification of this model was carried out with commercial finite element package ABAQUS, using the hardness measurement data from Hudson^[1] for its verification.

After the development and verification against existing measurement data, the microstructure model was implemented in a stand-alone software tool. Since the microstructure model was implemented with the thermal model together, it went through the same steps as the thermal model did. The details of the implementation, its structure, components, and usage are described in the final report for the thermal model^[2].

2.1 Technical Approach for Microstructure Model

2.1.1 An Overview

As stated in Section 1, in an ideal microstructure model for welding process, the weld metal and its HAZ need to be treated differently. However, because of the lack of established microstructure models for weld metal with the capability of predicting overall hardness, the grain growth component of HAZ microstructure model was slightly modified and applied to the weld metal. A second approach was later developed in order to improve the accuracy of hardness prediction for the weld metal.

In the sections below, the microstructure models and their implementations for HAZ and weld metal are described.

2.1.2 Microstructure Model for HAZ

Overall, the model takes a thermal cycle, i.e., temperature as a function of time, and the chemical composition of the material as inputs. The model then simulates the austenization, grain growth, and austenite decomposition as heating and cooling take place. At the end of the simulation, the final phase volume fractions and the hardness are determined. Three parts are included in the model: a thermodynamics part that calculates the phase transformation parameters, a grain growth part that determines the prior-austenite grain size, and the third part that simulates the austenite decomposition process. Emphasis is given to the grain growth model in this report since other parts of the model were well-documented in the references, for example, by Watt et al^[8].

Thermodynamics Calculation

In preparation for the calculation of grain growth and the ensuing austenite decomposition during cooling, a few important critical temperatures for phase transformation are needed. These include the A_{e3} temperature, the eutectoid temperature, A_{e1} , the bainite start temperature, B_S , the martensite start temperature, M_S , and the precipitate dissolution temperature. To calculate the first two temperatures, Li's^[7] approach is followed in the present approach to determine the equilibrium phase boundary. B_S and M_S are determined

using the Kirkaldy and Venugopalan empirical equations^[6]. The precipitate dissolution temperature is obtained with the Ashby/Easterling relation^[17]. These equations were documented in the references in details and are not presented here again.

Grain Growth

Following the original Ashby and Easterling grain growth model^[17], a few similar forms have been proposed. In general, all of them can be presented as the following:

$$\frac{dg}{dt} = \frac{k}{mg^{m-1}} e^{-Q/RT}$$

where g is the grain size, Q the activation energy for grain growth, T the temperature in Kelvin, k and m both empirical constants. While the grain growth calculation is very sensitive to the selections of Q , k , and m , no unique values for them have been agreed upon so far. Both Ashby et al^[17] and Watt et al^[8], for example, used the value of $m=2$; Ikawa et al.^[18] reported that $m=3$ was better to explain their measurements; Miranda and Fortes^[19] however, recommended the value of $m=3.17$ in their grain growth calculation for 2.25Cr-1Mo steel. In the current model, the value of m was evaluated according to the correlation approach by Chen and Wang^[14].

Austenite Decomposition

The original empirical equations developed by Kirkaldy and Venugopalan describe the reaction rates at which the austenite decomposes into its child products such as ferrite, pearlite, and bainite. For each reaction, the rate equation is characterized as:

$$\frac{dX}{dt} = B(G, t)X^p(1 - X)^q$$

where X is the volume fraction of the child product, B an effective rate coefficient, G the austenite grain size, and p and q semi-empirical coefficients. We followed the approach by Watt to implement the numerical algorithm based on the reaction rate equations by Kirkaldy and Venugopalan. The simulation starts with the heating first. As the temperature rises above the eutectoid temperature A_{e1} , austenitization starts; when the precipitate dissolution temperature is reached, the grain growth begins according to the above equation. Upon cooling, the grain growth continues until austenite decomposition takes place. Depending on the temperature, ferrite, pearlite, bainite, and martensite are formed at different stages. At the end of the simulation, the final volume fractions of each phase are determined. In order to calculate the hardness, the rule of mixtures is used. The component relationships for martensite hardness H_M , bainite hardness, H_B , and hardness for ferrite/pearlite, H_{FB} , used in this rule of mixtures are as the following^[8]:

$$\begin{aligned} H_M &= 127 + 949(C) + 27(Si) + 11(Mn) + 8(Ni) + 16(Cr) + 21\log V_r \\ H_B &= -323 + 185(C) + 330(Si) + 153(Mn) + 65(Ni) + 144(Cr) + 191(Mo) \\ &\quad + [89 + 53(C) - 55(Si) - 22(Mn) - 10(Ni) - 20(Cr) - 30(Mo)]\log V_r \\ H_{FP} &= 49 + 223(C) + 53(Si) + 30(Mn) + 12.6(Ni) + 7(Cr) + 19(Mo) \\ &\quad + [10 - 19(Si) + 4(Ni) + 8(Cr) + 130(V)]\log V_r \end{aligned}$$

where V_r is the cooling rate at 700°C and \log is the logarithm to base 10. The final total hardness is the averaged hardness weighted by each component's volume fraction.

2.1.3 Microstructure Model for Weld Metal

The microstructure model for the weld metal followed the same formulation as described in the previous section except for the grain growth model. The modification to the grain growth in weld metal is necessary because it goes through a solidification process and develops a unique columnar austenite grain structure as it cools down. The averaged prior austenite grain size in the weld metal, immediately after the solidification, is related to the chemical composition of the weld and the heat input of the welding pass according to Bhadeshia:

$$g = 64.5 - 445.8(C) + 139(Si) - 7.6(Mn) + 16HI$$

where g is the averaged grain size in μm , and HI is the welding heat input in kJ/mm .

An alternative approach for the weld metal was later implemented by correlating the hardness of the weld metal with its chemical composition and the cooling times T_{85} or T_{84} . The purpose of using this alternative approach was to improve the accuracy of hardness prediction by the microstructure model for the weld metal. A detailed discussion on this alternative approach will be presented later.

2.2 Numerical Implementation of Microstructure Model

The microstructure model described in the previous section was developed first using a commercial finite element package ABAQUS. After its successful development and verification against existing measurement data, it (together with the thermal model) was implemented in a stand-alone software tool.

In its ABAQUS implementation, two of the three components in the microstructure model, grain growth and austenite decomposition, were coded in an ABAQUS user subroutine. The volume fractions of constituents and hardness distribution were defined as nodal state variables in the subroutine in the finite element mesh.

In the stand-alone software analysis tool, the microstructure model was implemented in two components. The first component was for the thermodynamics calculation of phase transformation temperatures and kinetics reaction rates for austenite decomposition, and it was coded as a separate dynamically-linked library (DLL). The second component included the other two parts of the microstructure model, the grain growth and the austenite decomposition, and they were coded within the framework of the thermal model.

3 Verification and Applications of Microstructure Model

The previous sections have described the technical approach for the microstructure model for a multi-pass, multi-wire GMAW girth welds. Together with the thermal model, the

microstructure model was implemented in two different formats. The first one was through the use of commercial finite element package ABAQUS. After the verification of the procedure with ABAQUS was complete and the procedure proved to be effective, the model was implemented in a stand-alone analysis software tool.

In the process of development and implementations of the microstructure model, a number of sets of experimental data were used to calibrate and verify the procedure. The major data sets include:

- 1) The hardness measurement data by Hudson^[1];
- 2) The HAZ Gleeble simulation results; and
- 3) Experimental plate welds and X100 pipe girth welds.

These calibrations and verifications were performed to establish the microstructure model as a prediction tool for the microstructure and hardness evaluation of a girth weld.

In addition to its verification, the microstructure model was used to perform the virtual experiment in the effort to identify and quantify the welding essential variables.

In developing the alternative approach to weld metal hardness modeling, the weld metal Gleeble simulation results were used, and weld metal hardness measurements by others^[1] were collected to correlate the hardness with the composition and cooling times of the weld metal.

In the following subsections, the verifications of the microstructure model and its applications are presented.

3.1 Verification of Microstructure with Hudson’s Hardness Data

The microstructure model described in Section 2.1 was implemented first with finite element software ABAQUS. This subsection presents the predicted hardness results and some of their comparisons with the measurements by Hudson^[1].

The experimental measurements by Hudson had two series of data: (1) preheat variation trials and (2) process variation trials as they were called in the original work. The first series included girth welds made under different pre-heat temperatures. The second series included girth welds made with different P-GMAW variants, namely, single wire, tandem wire, and dual torch processes. For both trials, the external welding passes were made with 1.0mm Oerlikon Carbolfil NiMo-1 (0.9Ni 0.3Mo) consumable. The representative chemical composition of the weld metal is list in Table 1. Detailed information of the welding conditions for these girth welds can be found in Reference 1.

Table 1: Representative chemical composition of weld metal for pre-heat and process variation trials^[1].

Element	C	Mn	P	Si	Cr	Ni	Mo	Cu	Al	V	Nb	Ti
Weight %	0.080	1.640	0.008	0.650	0.070	0.850	0.320	0.140	0.005	0.013	0.008	0.050

Simulation Results for Preheat Variation Trials

This set of data was obtained using single wire P-GMAW process with an internal root pass, one hot pass, and five fill passes. The pipes were X100 grade with a diameter of 752 mm (30 inches) and a wall thickness of 19.05 mm (0.75 inches). For these welding experiments three preheat temperatures were used: room temperature (27°C), 100°C, and 180°C. The pipes were preheated to the respective temperatures before the welding of each pass. The chemical composition for the X100 pipe is listed in Table 2.

Table 2: Chemical composition of X100 pipe for pre-heat variation trials[1].

Element	C	Mn	P	Si	Cr	Ni	Mo	Cu	Al	V	Nb	Ti
Weight %	0.027	1.980	0.006	0.200	0.420	0.480	0.430	0.460	0.006	0.070	0.050	0.050

The through-thickness distributions of hardness along the center line of the girth weld are plotted in Figure 1. In general, both the prediction and the measurements show the expected trend, i.e., higher preheat temperature leads to softer weld. The overall distribution of the computed hardness distribution agrees with that of the experimental measurements. From the plots, it is demonstrated that the microstructure model was able to capture the trend of hardness variation as a function of welding parameters. To further illustrate the influence of the preheat temperature on the hardness of both weld metal and the HAZ, hardness contour plots for the three preheat temperatures are shown in Figure 2. These contours not only show that the overall predicted hardness decreases, they also reveal that the HAZ softening becomes more and more pronounced as the preheat temperature is increased. This phenomenon may have a significant implication for welding of X100 steel pipe. If the heat input is too low, high hardness may exist in both weld metal and HAZ regions and this could lead to potential problems. On the other hand, if the heat input or the preheat temperature is too high HAZ softening may also occur and potentially compromise the strength in the vicinity of a pipeline girth weld.

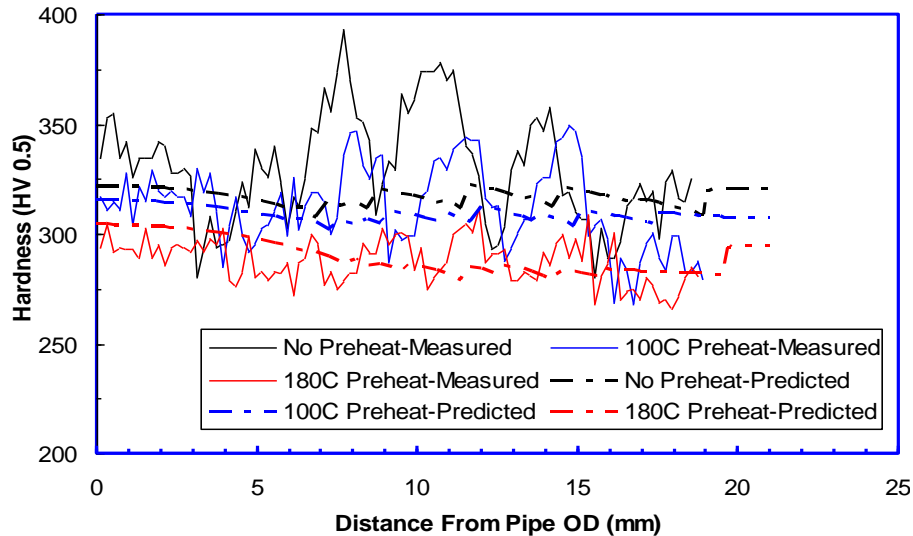


Figure 1: Measured and computed hardness distributions along the weld centerline for different preheat temperatures.

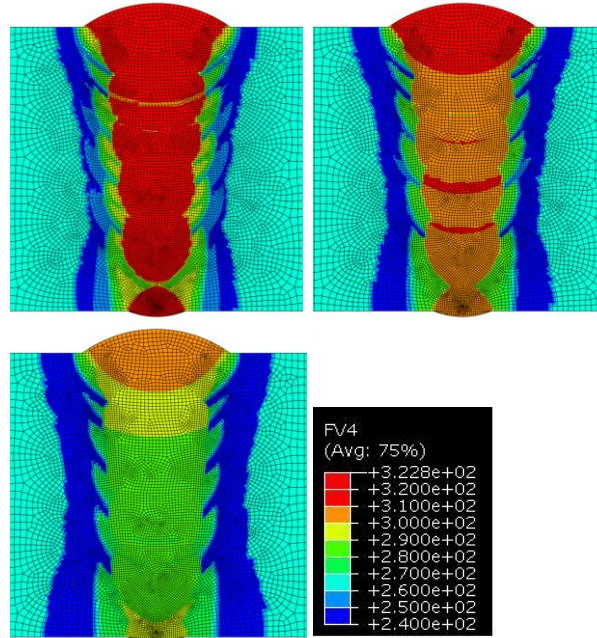


Figure 2: Hardness contours for different preheat temperatures. Top left: no preheat; top right: 100°C preheat; bottom left: 180°C preheat

Simulation Results for Process Variation Trials

This part of verification of the microstructure model focused on three different P-GMAW process variants, namely, single torch, tandem and dual torch. For these experiments the X100 grade pipes had a diameter of 914.4 mm (36 inches) and a wall thickness of 19.05 mm (0.75 inches). All three procedures used the same weld joint geometry design and the same preheat/inter-pass temperature of 100°C. The tandem wire consists of a single torch with two electrodes, arranged close together and feeding into the same weld pool (3.4 mm in this case according to Hudson). The dual torch process used two torches; each with a single wire that were fixed 80 mm apart (wire spacing). The chemical composition of the X100 pipe is listed in Table 3.

Table 3: Chemical composition of X100 pipe for process variation trials^[1]

Element	C	Mn	P	Si	Cr	Ni	Mo	Cu	Al	V	Nb	Ti
Weight %	0.066	1.910	0.008	0.100	0.020	0.540	0.270	0.300	0.020	0.006	0.030	0.013

Figure 3 plots the through-thickness distribution of the hardness at the girth weld centerline. The single wire process and the tandem wire process display very similar hardness profiles and values, both from the measurements and the predictions. The dual torch process, however, produced a much softer weld and HAZ, as indicated by both measurements and predictions. Again, the microstructure model was able to capture the trend of hardness variations under different welding processes. The exact hardness values by the prediction can be quite different from those of measured, as in the case of dual torch weld. Detailed examination of the prediction results indicated that under slow cooling conditions such as in dual torch welding, the reaction rates of ferrite can be overestimated if the initial grain size is small (5-10µm) and the grain growth is not significant. As a result, excessive amount of

local ferrite volume fraction and low hardness are predicted. Figure 4 shows the hardness contours for all the three processes. The dual torch process not only produced a much softer weld, its softened HAZ region is also much wider. This significant decrease in hardness for the dual torch process is due to the increase of so-called effective heat input. As documented in the experiment data, the heat input for each of the torches in the dual torch process variant was similar to that of the single wire process. Because the two torches were separated by a short distance (relative small delay time), the effective heat input was increased. The consequence for the weld metal when the trailing torch arrives is that the residual temperature field resulting from the leading torch is still quite high. This acts as a very high “distributed” preheat, and the residual temperature field leading to a very slow cooling time for the trailing torch. As a result, the hardness in both the weld metal and the HAZ are much lower.

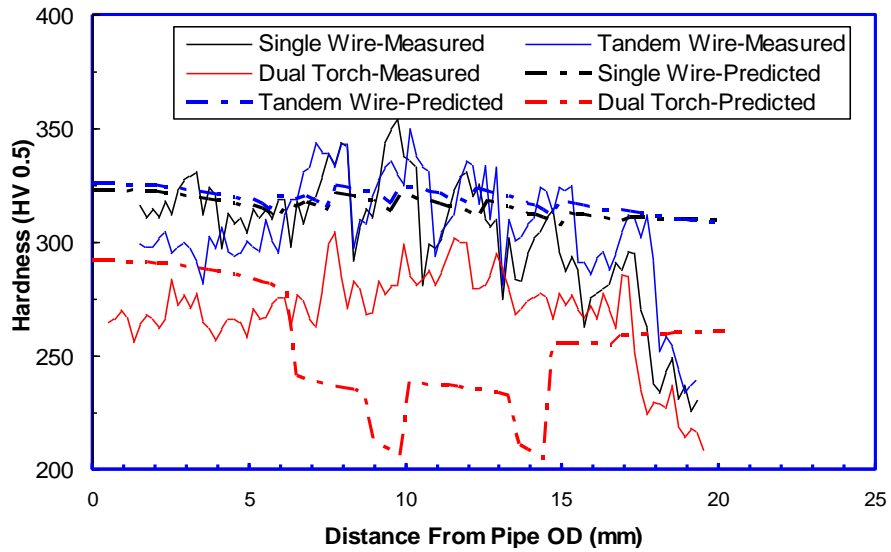


Figure 3: Transverse distributions of hardness along the centerline of girth weld for single wire, tandem wire, and dual torch processes.

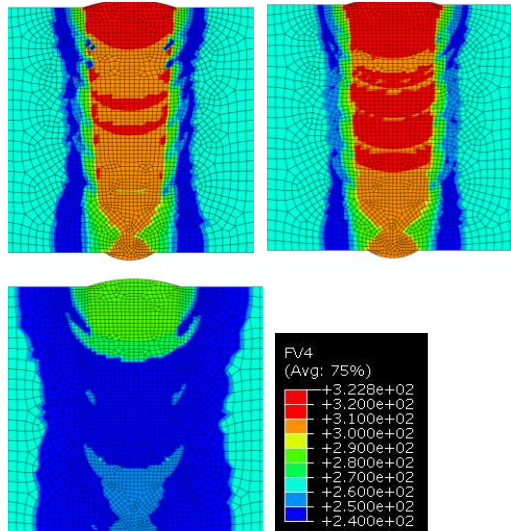


Figure 4: Hardness contours for different processes. Top left: single wire; top right: tandem wire; bottom left: dual torch.

3.2 Verification of Microstructure Model with HAZ Gleeble Simulation Data

In order to calibrate the microstructure model for its effectiveness in simulating the phase transformation in the HAZ, a set of Gleeble simulation tests were performed on one of the vintage X100 pipe steels at CANMET. For proprietary reasons, the chemical composition of this vintage X100 steel was not given. The Gleeble simulations were performed with six cooling times, $T_{85}=1.2, 3.0, 5.0, 10.0, 16.0,$ and 25.0 seconds, respectively. A typical simulation thermal cycle for $T_{85}=1.2$ s is demonstrated in

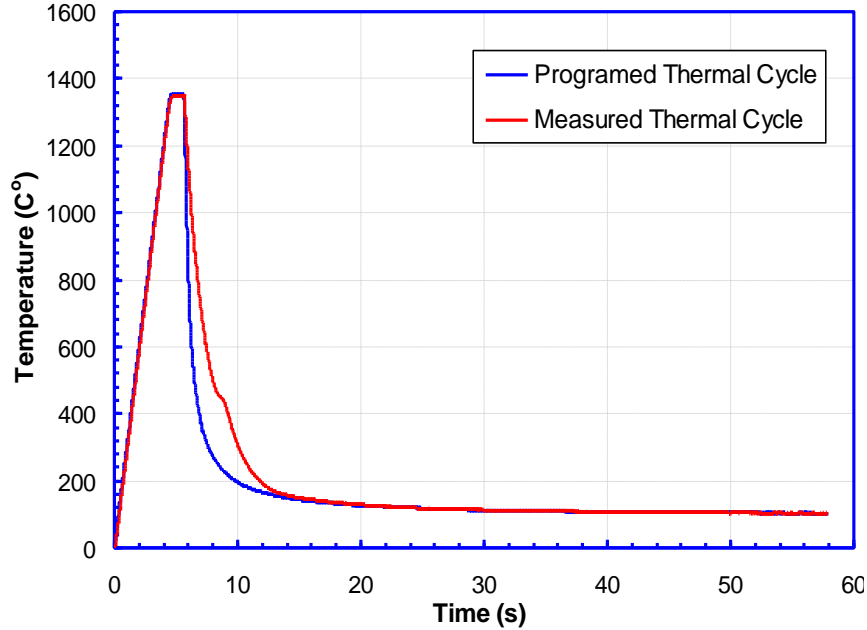


Figure 5: Gleeble simulation thermal cycle with $T_{85}=1.2$ s

In verifying the HAZ microstructure model against the Gleeble data, an independent module that only contains the HAZ microstructure model was produced from the integrated thermal-microstructure model codes. This independent module was able to read the measured thermal cycle data from the HAZ Gleeble test and perform the single-cycled microstructure simulation.

Table 4: Comparison of microstructure properties between HAZ Gleeble test and predictions by HAZ microstructure model (VF: volume fraction)

Sample #	T_{85} (s)	Estimated Grain Size (μm)	Martensite VF (%)		Bainite VF (%)		Hardness (VH)	
			Estimated	Predicted	Estimated	Predicted	Measured	Predicted
1	1.2	75	95.0	98.3	N/A	0.8	381	339
2	3	100	70.0	96.2	N/A	2.4	337	332
3	5	100	57.5	90.6	N/A	5.6	326	308
4	10	100	30.0	69.1	N/A	18.8	280	290
5	16	100	16.5	31.0	N/A	41.9	259	241
6	25	200	10.0	43.2	N/A	36.2	270	257

Table 4 lists the estimated and predicted final volume fractions of bainite and martensite and the Vickers hardness for the six Gleeble test cases. Also listed are the estimated prior-austenite grain sizes based on visual examination of the micrographs of the test samples. One observation from the table is that even though the prior-austenite grain size and the volume fractions of constituents from the Gleeble simulation results were estimated, the microstructure model was able to use the approximate information to predict the right trend of the hardness as a function of cooling time T_{85} . The over-prediction of martensite volume fraction may be attributed to the over-estimated grain growth. As pointed out earlier, in the microstructure model, large prior-austenite grain size reduces the production of ferrite and leads to more martensite in the final microstructure.

3.3 Verification of Microstructure Model with Plate Welds and Girth Welds

In further verifying the microstructure model, one plate weld made with a prototype welding consumable and one X100 pipe girth weld made under practical welding conditions were selected. The plate was obtained by flattening the pipe. The X100 pipe has an outside diameter of 36 in. and a wall thickness of 0.75 in. The detailed welding conditions for these two welds can be found in the final report for the thermal model^[2].

3.3.1 Plate Weld

The plate experimental weld was made with a prototype consumable named PT1 with no pre-heat or inter-pass heating. The welding parameters for the weld and the chemical composition for consumable PT1 are listed in Table 5 and Table 6 respectively.

Table 5: Averaged welding parameters for plate weld

Pass	Voltage (V)	Current (A)	Travel Speed (mm/min)	Heat Input (kJ/mm)
Hot Pass	25	188	1346.2	0.2
Fill Pass 1	24	185	508	0.5
Fill Pass 2	24	206	508	0.6
Fill Pass 3	23	194	508	0.5
Deep Fill	23	249	228.6	1.5

Table 6: Chemical composition of consumable PT1

Element	C	Mn	Si	Ni	Cr	Mo	II
wt%	0.08	1.5	0.5	1.6	0.3	0.5	0.04

From the welding parameters of Table 5, a unique feature of this experimental plate weld was that the weld was made with a low heat-input hot pass, followed with three moderate heat-input passes, and its final pass (deep fill) had a heat input three times as high as the three previous passes. The wide spread of heat inputs of the welding passes within a weld provided a benchmark to test the robustness for the integrated thermal-microstructure model.

Figure 6 shows the calculated hardness distribution for the plate weld. It demonstrates the wide HAZ softening region produced by the deep fill. It also captures the hardness bands due to reheating in the early fill pass region by subsequent weld passes. But its predicted values

of hardness in the deep fill region is questionable since much lower hardness values should be expected considering the relatively high heat input associated with the deep fill pass. This discrepancy between the predicted hardness values and the actual hardness in the weld is confirmed in Figure 7. While the model correctly captures the hardness variation profile along the weld centerline, the predicted hardness values in the deep fill region are much higher than the measured ones. Considering that the deep fill pass is the last pass and its weld metal does not experience any reheating, the overestimated hardness by the model may be due to its inaccuracy of phase transformation kinetics.

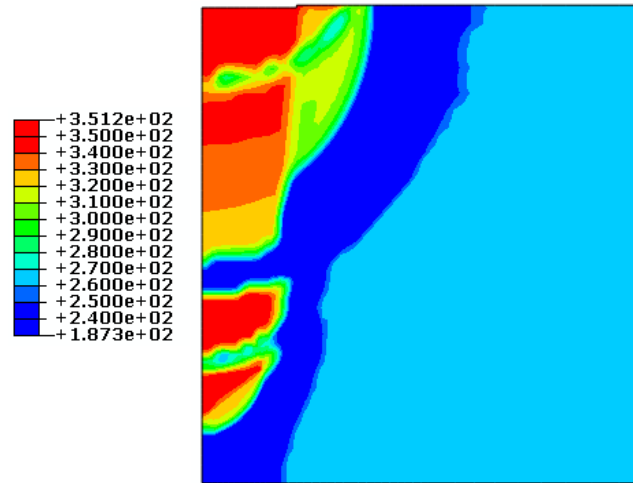


Figure 6: Predicted hardness distribution for plate weld.

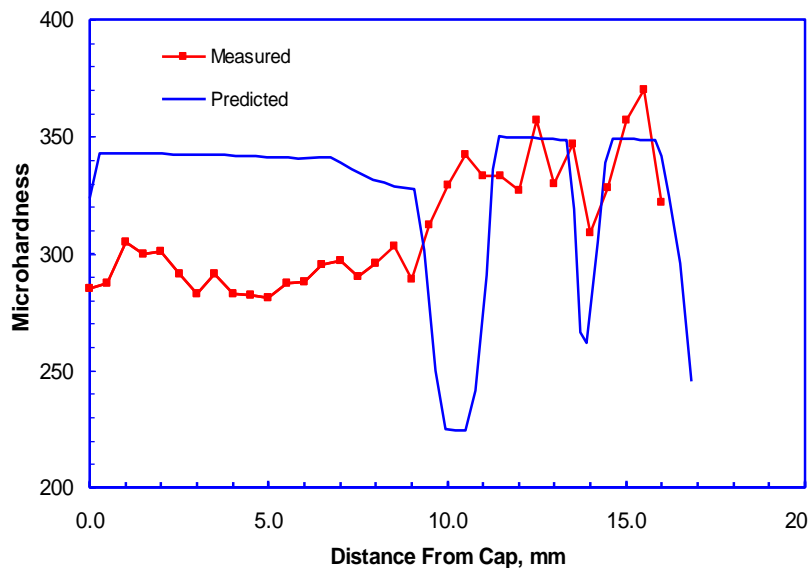


Figure 7: Measured and predicted hardness profiles along weld centerline for plate weld.

3.3.2 Pipe Girth Weld

The pipe girth weld was made during the first round welding with a single torch P-GMAW process. The chemical compositions of the pipe and the weld metal are listed in Table 7. The welding parameters are listed in Table 8.

Table 7: Chemical compositions of X100 pipe and weld metal.

Element	C	Mn	Si	Ti	Cr	Mo	Ni	P	Al	Cu	V	B	Nb	W
Weld Metal	0.097	1.390	0.580	0.038	0.050	0.350	0.960	0.013	0.005	0.134	0.003	0.000	0.003	0.027
X100 Pipe	0.068	1.860	0.110	0.009	0.030	0.270	0.530	0.006	0.042	0.310	0.002	0.000	0.029	0.015

Table 8: Averaged welding parameters for the girth weld.

Pass No.	Welding Current (A)	Welding Voltage (V)	Wire Feed Speed (m/min)	Travel Speed (mm/min)	Heat Input (kJ/mm)
Hot Pass	199.3	20.6	10.6	1342.0	0.18
Fill Pass 1	199.6	22.0	10.6	505.7	0.52
Fill Pass 2	198.8	22.5	10.6	505.6	0.53
Fill Pass 3	198.7	22.4	10.6	505.7	0.53
Fill Pass 4	198.4	22.5	10.6	505.8	0.53
Fill Pass 5	198.4	22.5	10.6	455.4	0.59
Cap Pass	147.6	23.5	8.2	445.2	0.47

The measured micro-hardness map and the predicted hardness distribution are plotted in Figure 8. Again, the model was able to capture the bands of hardness produced by the reheating of subsequent weld passes, though the absolute values of the predicted hardness are higher in general than the measured values. The comparison between the predicted and measured hardness distributions suggests that in a real situation, the hardness of early passes of the weld would decrease after the reheating by the later passes. The amount of this decrease in hardness depends on the temperature profile of the reheating, in particular, the peak temperature and the cooling rate. With different peak temperatures, the reheating thermal cycles can cause microstructure changes in the regions where full re-austenitization (supercritical reheating), intercritical reheating, or subcritical reheating occurs. Based on this rationale, it is concluded that improvements of the microstructure model in the areas of re-austenitization, intercritical phase transformation, and tempering would certainly increase the prediction accuracy.

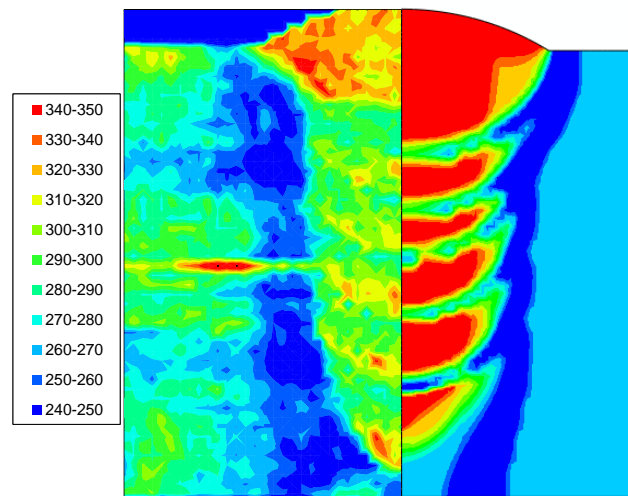


Figure 8: Measured micro-hardness (left) vs. predicted hardness distribution (right) in a girth weld.

3.4 Virtual Experiments and Identification of Essential Variables

The essential part of the project research work was a complete assessment of essential variables and improved understanding of the factors influencing properties of high strength steel pipeline girth welds and their performance.

After the integrated thermal-microstructure model went through three rounds of calibrations and verifications against the measured thermal cycles and hardness data, it proved to be accurate in predicting thermal cycles for multi-pass, multi-wire GMAW and reasonably accurate in predicting the trend of hardness. Consequently, the thermal model was used as the primary tool to conduct a virtual experiment to identify the welding essential variables. Details of the design, execution, and thermal and microstructure simulation results of the virtual experiment were presented in the topical report for the thermal model.

The test matrix of the virtual experiment was designed and expanded by changing some of the welding parameters while keeping others the same. These welding parameters are:

- 1) Bevel offset
- 2) Pre-heat/inter-pass temperature
- 3) Torch configuration
- 4) Welding procedure
- 5) Electrode type

The bevel offset values included 2.3 mm (0.09 inches) and 2.8 mm (0.11 inches). Three levels of pre-heat and interpass temperatures were considered: 27°C, 100°C, and 180°C. The torch configuration included single and dual torches. Three electrode types were considered in the experiments: a NiMo type, Prototype 1, and Prototype 2. The term “welding procedure” here was defined by the welding sequence and its associated heat inputs for each pass and its dependency on the other welding parameters. In total forty cases were included in the test matrix.

After the test matrix was finalized, forty input files, one for each experiment case, were compiled according to the welding conditions. The simulations of the forty cases were then executed on a 32-bit Microsoft Windows personal computer. For each pass, two key pieces of information from the outputs were selected to represent the overall properties of the welding process and the weld. The first one is the cooling times T_{85} and T_{84} of the thermal cycle at the HAZ of fill pass 1; the second overall properties are the hardness profile along the weld centerline and the hardness profile across the weld at the middle plane of the pipe.

The microstructure data from the virtual experiment were used directly in the sensitivity study to identify the welding essential variables. The summary of the microstructure data and how they were used in the process were covered in a different topical report of the project, Report 278-T-07.

4 Concluding Remarks

For the welding of X100 linepipe steels, the identification of essential variables is critical to establish a viable range of welding conditions so that the required mechanical properties of the weld can be met. In addition to the conventional essential variables such as heat input, pre-heat and inter-pass temperatures, electrode consumable, and shielding gas, etc., the multi-wire GMAW variants added more welding variables and some of them may emerge as essential variables.

In the effort of identifying these essential variables, an integrated thermal-microstructure model has been developed and verified against a large amount of measured thermal cycle and microstructure data. This model was also implemented through finite element method as a stand-alone analysis software tool.

4.1 Thermal-Microstructure Modeling of Multi-Pass, Multi-Wire P-GMAW Process

The thermal-microstructure model was developed and verified against a number of experimental data sets, including the data by Hudson, the measurement data from the first round welds, and the measurement data from the second round welds, the HAZ Gleeble simulation results. The model can simulate not only the traditional single-wire GMAW process but also the multi-wire GMAW variants. For the microstructure model, it proved that it can predict the trend of hardness in GMAW girth weld as a function of welding parameters although its accuracy needs improvement.

After its calibrations and verifications, the thermal-microstructure model was used in the effort of identifying essential variables. It served as the primary analysis tool in performing the virtual experiments.

4.2 The Integrated Thermal-Microstructure Analysis Tool

Because the thermal-microstructure model was implemented as a stand-alone software tool, it offers several advantages compared to using a commercial finite element package:

- 1) It automated a complicated modeling procedure, including the integration between the thermal model and the microstructure model.
- 2) As the direct results of procedure automation, the analysis tool is highly efficient and not error-prone at all compared to a manual process of model development;
- 3) Because it is written in generic finite element method, new features can be readily incorporated and implemented in the procedure.

5 References

- 1 Hudson, M., “*Welding of X100 Linepipe*,” Ph. D. Thesis, Cranfield University, Cranfield, UK, 2004.
- 2 Chen, Y., Wang, Y.-Y., Quintana, M.A., Rajan, V.B. and Gianetto, J.A., “Thermal Model for Welding Simulations”, Final Report 278-T-07 to PHMSA per Agreement #DTPH56- 07-T-000005, September 2011.
- 3 Yurioka, N., Okumura, T., and Kasuya, T., and Cotton, H.J.H., “Prediction of HAZ Hardness of Transformable Steels,” *Metal Construction*, 19(4), pp 217R-223R, 1987.
- 4 T. Kasuya, Y. Hashiba, and M. Okumura, “Methods for Predicting Maximum Hardness of Heat-Affected zone and Selecting Necessary Preheat Temperature for Steel Welding,” *Nippon Steel Technical Report No. 65*, April 1995.
- 5 T. Kasuya and Y. Hashiba, “Carbon Equivalent to Assess Hardenability of Steel and Prediction of HAZ Hardness Distribution,” *Nippon Steel Technical Report No. 95*, January 2007.
- 6 Kirkaldy, J. S. and Venugopalan, D., in *Phase Transformation in Ferrous Alloys* (Edited by Marder, AR and Goldstein, JI), Philadelphia, pp. 125-48, October, 1983.
- 7 Li, M. V., Niebuhr, D. V., Meekisho, L. L., and Atteridge, D. G., “A computational model for the prediction of steel hardenability,” *Metallurgical and Materials Transactions B*, Vol. 29, No. 3, pp. 661-672, 1998.
- 8 Watt, D. F., Coon, L., Bibby, M. J., Goldak, J. A., and Henwood, C., “An algorithm for modeling microstructural development in weld heat affected zones,” *Acta Metal*, Vol. 36, No 11, pp. 3029-3035, 1988.
- 9 Oddy, A. S., McDill, J. M. J., and Karlsson, L., “Microstructural Predictions Including Arbitrary Thermal Histories, Reaustenization and Carbon Segregation Effects,” *Canadian Metallurgical Quarterly*, Vol. 35, No. 3, pp 275-283, 1996
- 10 Oddy, A. S. and McDill, J. M. J., “Numerical Prediction of Microstructure and Hardness in Multi-cycle Simulation,” *Journal of Materials Engineering and Performance*, Vol. 5(3), 1996.
- 11 Borjesson, L and Lindgren, L., “Simulation of Multipass Welding with Simultaneous Computation of Material Properties,” *Journal of Engineering Materials and Technology*, Vol. 123, No. 1, pp. 106-111, 2001.
- 12 Bhadeshia, H. K. D. H., Svensson, L. E., in *Mathematical Modeling of Weld Phenomena*, H. Cerjak and K. E. Easterling , eds., Institute of Materials, London, pp. 109-180, 1993.
- 13 Nunzio, P. E., Cesile, M. C., Anelli, E., and Poli, A., “A physical model for microstructure predictions in multi-pass welding of seamless pipes,” *Proc. Materials Solutions Conference 2002-International Symposium on Micro-alloyed Steels*, edited by R. I. Asfahani, R. L. Bodnar, and M. J. Meervin, 7-9 October 2002, Columbus, OH, ASM International, pp. 148-156, 2002.
- 14 Chen, Y. and Wang, Y.-Y., “Microstructure Modeling of HAZ Softening in Microalloyed High Strength Linepipe Steels,” *Proceedings of the 17th International Offshore and Polar Engineering Conference (ISOPE 2007)*, Lisbon, Portugal, July 1-6, 2007.
- 15 Nolan, D., Sterjovski, Z., Grace, P., and Bruce, W., “Effect of Steel Composition on Microstructure and Hardness of the Heat-Effectuated Zone for In-Service Welding of

- Pipelined,” International Pipeline Integrity and Repair Conference, Sydney, March 2004, Paper 11.
- 16 Nolan, D., Sterjovski, Z., and Dunne, D., “Hardness prediction models based on HAZ simulation for in-service welded pipeline steels,” *Science and Technology of Welding and Joining*, Volume 10, No. 6, pp681-694, 2005.
 - 17 Ashby, M.F., and Easterling, K.E., “A First Report on Diagrams of Microstructure and Hardness for Grain Growth in Welds,” *Acta Metall.*, Vol 30, No 11, pp1969-1978, 1982.
 - 18 Ikawa, H., Oshige, H., Noi, S., Date, H., and Uchikawa, K., *Trans. Jpn. Weld. Soc.*, Vol 9, pp47-50, 1978.
 - 19 Miranda, R.M. and Fortes, M.A. “Austenite Grain Growth, Microstructure and Hardness in the Heat-Affected Zone of a 2.25Cr- 1Mo Steel,” *Mater. Sci. Eng.*, Vol 108A, pp1-8, 1989.